ACS APPLIED MATERIALS & INTERFACES

Research Article

www.acsami.org

Ce(III) Doped Zr-Based MOFs as Excellent NO_2 Adsorbents at Ambient Conditions

Amani M. Ebrahim and Teresa J. Bandosz*

Department of Chemistry, The City College of New York and The Graduate School of CUNY, 160 Convent Avenue, New York, New York 10031, United States

ABSTRACT: New hybrid cerium modified zirconium based metal−organic frameworks (MOFs) were synthesized. The as-received materials were evaluated as adsorbents of NO_2 in either moist or dry conditions. The surface of the initial and exhausted samples was characterized using XRD, SEM-EDX, nitrogen adsorption, thermal analysis, and FTIR. It was found that the addition of Ce^{+3} slightly affects the growth of the framework and introduces new features to Zr-MOF. The shapes of the octahedral crystals are changed, and they are interwoven with rod-flake-like sheets. The extent of the interconnection, and thus the extent of the hybrid MOF formation, depends on the Zr to Ce ratio. The alterations in the surface chemistry and texture are reflected in the amount of NO_2 adsorbed. The narrow pore channels present in these new materials enhance adsorption in either moist or dry conditions. The amount of NO_2 adsorbed on the Ce-doped MOF increases over 25% in dry conditions in comparison with the unmodified MOF. Exposure of Ce-UiO-66 to NO_2 results in a development of porosity. Regardless the conditions, the XRD patterns indicate the stability of this new hybrid MOF upon NO_2 adsorption. Interactions of NO_2 with MOF result in the formation of nitrate and nitrite species associated either with metals or with organic ligands.

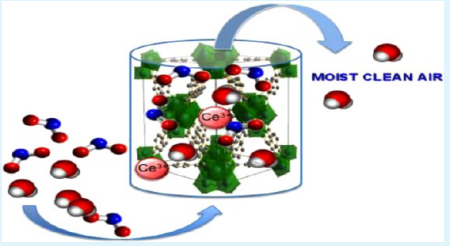

KEYWORDS: *Zr-MOF, metal doping, Ce^{+3} redox cycle, NO_2 adsorption, air filtration, moist conditions*

INTRODUCTION

Pollution issues and environmental concerns have led to the development of various techniques of air purification. Whether it is the abatement of the environmentally detrimental gases from source or their removal from air via adsorption processes, a scarcity in diverse and efficient materials continues to exist. The toxic gases of the NO_x family present in the atmosphere consist of mostly nitrogen monoxide (NO) and nitrogen dioxide (NO_2). Nitrogen dioxide has a higher level of toxicity than NO. It is corrosive and causes severe damage to materials, even at low concentrations.

Metal−organic frameworks (MOFs) have become extensively studied in the field of gas separation. Not only do MOFs have high specific surface areas and porosity, but they also have interesting and tunable topologies. Owing to the scarcity in renewable sources of energy, the studies on these crystalline porous networks have primarily focused on their ability to store hydrogen for energy usage.[1−5] The synthesis of MOFs involves many metals and organic linkers leading to the formation of either an acidic or basic crystalline porous MOF network. Such diversity of approaches allows researchers to tailor the chemistry of their MOF, for specific applications. For instance, Mg-MOF-74, a basic MOF, was shown to have high affinity for CO_2 and CH_4 adsorption.[6] Likewise, MOF-5, a Zn based acidic MOF, showed good hydrogen storage capabilities.[7]

Center cavities of various shapes in MOFs are obtained by using the same ligand and varying the metal, which changes the porosity of the final products. For example, Saha and coworkers reported the synthesis of four different MOFs from a BTB ligand and four trivalent metals (Al, Cr, Fe, Ga). They stated that the amount of hydrogen stored decreased in the following order Cr >Al >Ga>Fe.[8]

Even though MOFs have been considered as separation/storage media for H_2 and other nontoxic gases, their properties have made them also useful candidates to host toxic molecules harmful to the environment. A basic MOF MIL-53(Al) was used for the separation of CO_2 and H_2S from biogas.[9] The acidity as well as additional properties such as a high specific surface area and uniform micropore size distribution of MOF-177 (12.7 Å median pore diameter) and of MOF-5 (13 Å pore width) have been shown as important features for the efficient removal of NH_3 at various pressure ranges.[10] Petit and coworkers performed extensive studies on the reactive adsorption of ammonia on HKUST-1 and graphite oxide composites[11−13] as well as on MOF-5 hybrids with graphite oxide.[14,15] HKUST-1 was indicated as a diverse reactive adsorbent for acidic gases (H_2S and NO_2).[16] In these adsorption processes, however, the MOF structure is severely destroyed[16] which gives concerns to its reusability, and it thus creates the main drawback for this particular application.

Recently, new MOFs, UiO (The University of Oslo): UiO-66 and UiO-67, were synthesized and showed high chemical and thermal stability.[17] Previously, we have shown the performance of these zirconium-based MOF as adsorbents of NO_2 at ambient conditions.[18] The diversity in the adsorption capacity of these materials was linked to the presence of

Received: June 13, 2013
Accepted: October 7, 2013
Published: October 7, 2013

different ligands, determining the textural properties. The large ligand 4,4′-biphenyl-dicarboxylic acid, BDPC, present in UiO-67 results in a greater specific surface area and pore size than those of UiO-66, where BDC, benzene-1,4-dicarboxylic acid, is present. UiO-67 favored the retention of NO_2 in the presence of moisture, while similar adsorption performance in dry conditions was observed for both UiO-66 and UiO-67. NO_2 dissolved in the water film formed HNO_3, which enhanced the NO_2 adsorption capacity of UiO-67 under humid conditions by the nitration of the biphenyl rings present in BDPC.

Several studies have focused on studying the effect of introducing foreign metals of various oxidation states to the MOF framework on gas adsorption.[19−22] It was concluded that metal doping increases a gas uptake by providing additional sites for adsorption. For example, doping of MIL-53(Al) with a suitable amount of Li^+ enhanced the amount of hydrogen adsorbed from 1.66 to 1.84 wt %.[23] Moreover, incorporation of Li^+ cations to IRMOF-14 increased hydrogen adsorption at ambient temperatures.[24] Chu and coworkers extensively studied MOF-5 doped with Na^+, K^+, and Li^+ and found an increase in H_2 uptake in comparison with that on the parent MOF-5.[25] Li^+ cations incorporated into MOF have also been shown as positively affecting CH_4 and CO_2 separation.[26] Even though numerous studies have been focused on applications of MOF for energy storage, the implication of doping cationic species in MOFs has not been extensively studied for toxic gas adsorption.

The objective of this paper is the evaluation of the performance of new Ce^{+3} doped Zr-MOFs as adsorbents of NO_2 at ambient conditions. The surface chemistry and textural features of these materials are analyzed and linked to their adsorption performance in both moist and dry conditions. Not only should the incorporation of Ce^{+3} species provide the well-known redox phenomenon,[27,28] but it should also increase the number of active sites, which can favor NO_2 adsorption .

EXPERIMENTAL SECTION

Materials. All chemicals *N*,*N*-dimethylformamide (DMF, 99%), benzene-1,4-dicarboxylic acid (BDC, 98.9%), 4,4′-biphenyl-dicarboxylate (BDPC, 98.9%), dichloromethane (DCM, 99%), zirconium tetrachloride ($ZrCl_4$), and cerium trichloride heptachloride ($CeCl_3 \cdot 7H_2O$) were supplied by either Sigma-Aldrich, VWR, or Alfa Aesar and used without further purification.

Synthesis of Cerium-Doped Zr-MOF. The synthesis of Zr-MOFs was carried out following ref 12 with some amendments.[18] UiO-66(Zr) was prepared by dissolving 10 mmol of both zirconium tetrachloride, $ZrCl_4$, and BDC in 250 mL of DMF. The stoichiometirc ratio of Ce:Zr was 1:1. $CeCl_3$ and $ZrCl_4$ were used. Cerium trichloride heptahydrate (10 mmol) was stirred in DMF (50 mL), and then the $CeCl_3$ solution was transferred into the $ZrCl_4$/BDC solution and stirred for an additional 30 min. In the next step, the reagents were transferred to a 500 mL round bottom flask, and 50 mL of DMF was added. The system was heated at 120 °C under shaking for 24 h. A resulting white product was filtered off, washed with DMF, to remove the excess of an unreacted organic linker, and immersed in a dichloromethane solution for solvent exchange. The sample was again filtered and dried at 110 °C under vacuum for 24 h. The same procedures were followed for the synthesis of UiO-67, but BDPC was used as an organic linker. The as-synthesized hybrid materials are referred to as Ce-UiO-66 and Ce-UiO-67.

NO_2 Breakthrough Capacity. The NO_2 breakthrough capacities were measured in dynamic conditions using a laboratory-scale fixed-bed system at room temperature. In a typical test, 1000 ppm NO_2 in nitrogen diluted with air passed through a fixed bed of an adsorbent with a total inlet flow rate of 225 mL/min. The adsorbents were well mixed with 2 mL of nonreactive glass beads (diameter 0.5−1 μm) to obtain a homogenous bed and then well packed into a glass column (internal diameter 9 mm). The concentrations of NO_2 and NO in the outlet gas were measured using an electrochemical sensor (RAE Systems, MultiRAE Plus PGM-50/5P). The adsorption capacity of each adsorbent was calculated in milligrams per gram of adsorbent bed by integration of the area above the breakthrough curve. The tests were conducted in both moist (relative humidity 71 %) and dry (01−1% humidity) conditions by diluting NO_2 with air. The measurements were stopped at the concentrations of NO_2 and NO of 20 and 200 ppm, respectively (the limits of the gas sensors). After the breakthrough tests, all samples were exposed to a flow of carrier air only (180 mL/min) to evaluate the strength of NO_2 adsorption. The suffix -ED is added to the name of the samples after exposure to NO_2 in dry conditions, and -EM for samples after exposure to NO_2 in moist conditions.

Surface pH. The samples were first dried, then a 0.2 g sample of a dry adsorbent was added to 10 mL of deionized water, and the suspension was stirred overnight to reach equilibrium. Then the pH was measured using a Fisher Scientific Accumet Basic pH meter.

Adsorption of Nitrogen. Nitrogen isotherms were measured at −196 °C using an ASAP 2010 (Micromeritics) instrument. Before each analysis, initial and exhausted samples were dried and degassed at 120 °C. The surface area, $S_{BET,}$ the total pore volume, V_t, the micropore volume, V_{mic}, (calculated from the *t*-plot), and the mesopore volume, V_{mes}, were calculated from the isotherms. Pore size distributions were calculated using density functional theory.[29]

SEM-EDX Analysis. Scanning electron microscopy (SEM) and electron-dispersive X-ray (EDX) spectroscopy were performed on a Zeiss Supra 55 instrument with a resolution of 5 nm at 15 kV. For EDX spectroscopy, the analysis was done at magnification 1.6K and 3.7K. The contents of elements on the surface were calculated based on the means of three different single-point analyses. Analyses were performed on a sample powder previously dried. For some samples, a sputter coating of a thin layer of gold was performed to avoid specimen charging.

ICP. The evaluation of the cerium and zirconium content was done using a Varian MPX ICP instrument at Asbury Carbon (Asbury, NJ).

XRD. To obtain crystallographic structure of the materials, X-ray diffraction (XRD) was employed. Using standard powder diffraction procedures, the adsorbents (fresh and exhausted) were ground with DMF in an agate mortar, smear mounted onto a glass slide, and XRD was measured on a Philips X′Pert X-ray diffractometer using Cu Kα radiation with a routine power of 1600 W (40 kV, 40 mA)

Thermal Analysis. Thermogravimetric (TG) curves and their derivatives (DTG) were obtained using a TA Instruments thermal analyzer, Q600. The samples (initial and exhausted moist and dry) were previously dried in oven at 100 °C to remove moisture and then heated up to 1000 °C, with a heating rate of 10 °C/min under a nitrogen flow of 100 mL/min.

FTIR. Fourier transform infrared (FTIR) spectroscopy was carried out using a Nicolet Magna-IR 830 spectrometer using the attenuated total reflectance method. The spectrum was generated, collected 32 times, and corrected for the background noise. The experiments were done on powdered samples.

RESULTS AND DISCUSSION

For the sake of clear discussion, some results from our previous work addressing UiO-66 and UiO-67[18] are included in this paper in order to evaluate the effects of Ce^{+3} doping on the final properties of the modified MOF frameworks and on their adsorptive performance.

The XRD patterns for the UiO series with and without the incorporation of Ce(III) are shown in Figure 1. The main diffraction peaks specific to UiO-67 and UiO-66 are clearly visible for the Ce doped materials.[30−32] This indicates that the incorporation of Ce^{+3} does not totally alter the crystal growth of the UiO units. On the diffraction pattern for Ce-UiO-67, the position of the most intense peak at around $2\theta = 5.8°$ is slightly

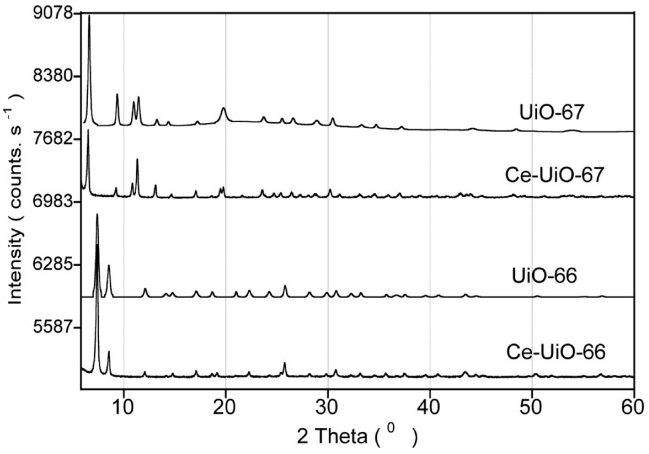

Figure 1. XRD patterns for the UiO series of samples with and without the incorporation of Ce(+3).

shifted to a higher angle. Moreover, the incorporation of Ce^{+3} leads to a decrease in the intensity of peaks at 2θ 10° and 20° and in the more flat baseline of the latter peak. New and distinct peaks are revealed on the diffraction pattern for Ce-UiO-67, and they show the structural effect of the incorporation of Ce^{+3} in the Zr-MOF matrix. They might correspond to the presence of several Ce species, such as $Ce(OH)_3$, $Ce(CO_3)_3$, and CeO_2.[33,34] It is hypothesized that these new features are the result of the interactions of Ce with the Zr−O center or the organic linker via π-complexation or a chelation process. Moreover, it is possible that Ce^{+3} is a site of a crystal growth. For Ce-UiO-66, minute changes are observed on the X-ray diffraction pattern in comparison with that of UiO-66. Nevertheless, some of the peaks characteristic for the latter sample decrease in their intensity or completely disappear, and the most prominent change is observed at the small diffraction angles (2θ = 9.9°). The results suggest that different chemistries of the ligands have marked effects on the extent of the structural alterations caused by Ce (III) doping into UiO-66 and UiO-67.

The effects of Ce^{+3} doping on the morphology of the UiO materials was further investigated, and the SEM images of the parent and Ce-doped UiO samples are presented in Figure 2. Here, significant differences in morphology as well as in crystal structure are seen when compared to the parent UiO materials, for which the crystals exhibit octahedral shape (Figure 2A and D). After doping, the crystal shape and geometry change (Figure 2B, C, E, and F). The particles are agglomerated round flakelike sheets, and it appears that if there still are well-defined crystals they are either covered or interwoven with the round flakelike units. Doping with Ce^{+3} either inhibits the complete Zr-MOF growth or disturbs the interactions between the Zr-metallic centers and the organic ligands. Moreover, cerium can be also a metallic center binding with ligand. Perhaps, the semicrystalline flakelike sheets are hybrids of Ce-MOF and Zr-MOF. This hypothesis is supported by the fact that the overall XRD patterns for UiO are preserved. The extent of agglomeration is more pronounced for Ce-UiO-67 (Figure 2E, F), where the greater changes in the XRD patterns are visible as compared to that of Ce-UiO-66 (Figure 2B, C). It is interesting to note that the particles in Ce-UiO-66 seem more flake/sheetlike than those present in Ce- UiO-67.

The elemental maps for the different UiOs doped with Ce^{+3} are presented in Figure 3. The surfaces of doped UiO-66 and UiO-67 are composed of oxygen, zirconium, and cerium. It is observed that, in both Ce-UiO-66 and Ce-UiO-67, cerium seems to be favorably linked to the zirconium containing crystals present in these MOFs. This metal is evenly distributed on the external surface of both materials analyzed by the EDX method. An interesting observation is a marked association of cerium with oxygen visible in the elemental maps for Ce-UiO-66. This indicates the heterogeneity of our materials and it further supports our hypothesis of a partial growth of Ce-MOF crystals either within or on the external corners of the Zr-MOF framework.

Even though the ratio of Zr to Ce was kept constant during the synthesis, different effective chemical compositions are detected by EDX analysis. Apparently, the ratio of zirconium to cerium seen on the surface is lower in Ce-UiO-66 (Zr/Ce = 8) than that in Ce-UiO-67 (Zr/Ce = 46). Thus, noncoordinated cerium species were washed away during filtration, and this process was much more pronounced for the latter sample. The high content of cerium in Ce-UiO-66 can be linked to the presence of a hybrid of Ce-MO/Zr-MOF structure seen on the SEM images of this material where a favorable dispersion of cerium with oxygen containing species was found. The ICP analysis of chemical composition follows the trend observed on the EDX maps. The content of cerium in the ashed Ce-UiO-66 and Ce-UiO-67 is 13.3% and 7.09%, respectively.

Additional information on the effect of Ce^{+3} doping on UiO chemistry is provided by the FTIR analysis. The spectra for MOFs with and without cerium doping are presented in Figure 4. Predictable peaks in UiO-67 representing various vibrations and stretching of the functional groups present in the BDPC ligand appear. The vibrations of the carboxylate groups present on the linker BDPC are seen at 1290 and 1430 cm^{-1}, and 1600−1640 cm^{-1}.[18,35] Even though the incorporation of cerium into the UiO-67 framework is not clearly seen on its FTIR spectrum, nonetheless, a small band at 1650 cm^{-1} appears. Moreover, a slight change in the band at 650 cm^{-1} is observed. This band is linked to the interactions of Ce^{+3} with the carbon moiety (COOH) in the BDPC ligand. For UiO-66, the weak band around 1650 cm^{-1} represents the stretching vibrations of C═O in the carboxylic acid present in BDC.[32] Typical bands representing the O−C−O asymmetric stretching in the BDC ligand are seen around 1600 cm^{-1}. The small bands at around 1540 cm^{-1} represent the typical vibration present in a C═C of a benzene ring, while the more intense band around 1400 cm^{-1} is linked to the O−C−O symmetric stretching in the carboxylate group of the BDC ligand.[18] The C−H vibration in the BDC ligand is visible at 780 and 810 cm^{-1}. Small broad bands at around 710 cm^{-1} are a result of the OH bending, C═C stretching, and OCO bending in the BDC ligand.[36] Unlike the minimal spectral changes seen in UiO-67 doped with Ce^{+3}, the effect of the cerium incorporation is clearly visible in Ce-UiO-66, where a new band at about 1645 cm^{-1} is revealed. We relate its appearance to the metallic coordination of Ce^{+3} species with the carbonyl group (C═O) present in the BDC ligand. Additional small changes in the overall spectrum for Ce-UiO-66 are also seen at lower wave numbers. They are due to the Ce−O stretching and Ce−O−C vibration in the MOF.[37] They indicate the formation of Ce-MOF or hybrid Ce/Zr-MOF as a result of cerium interactions with the BDC ligands.

The effect of the Ce^{+3} incorporation to the MOF framework is clearly visible in the parameters of the porous structure calculated from the nitrogen adsorption isotherms (Table 1). The N_2 isotherms (not shown here) indicate the microporous

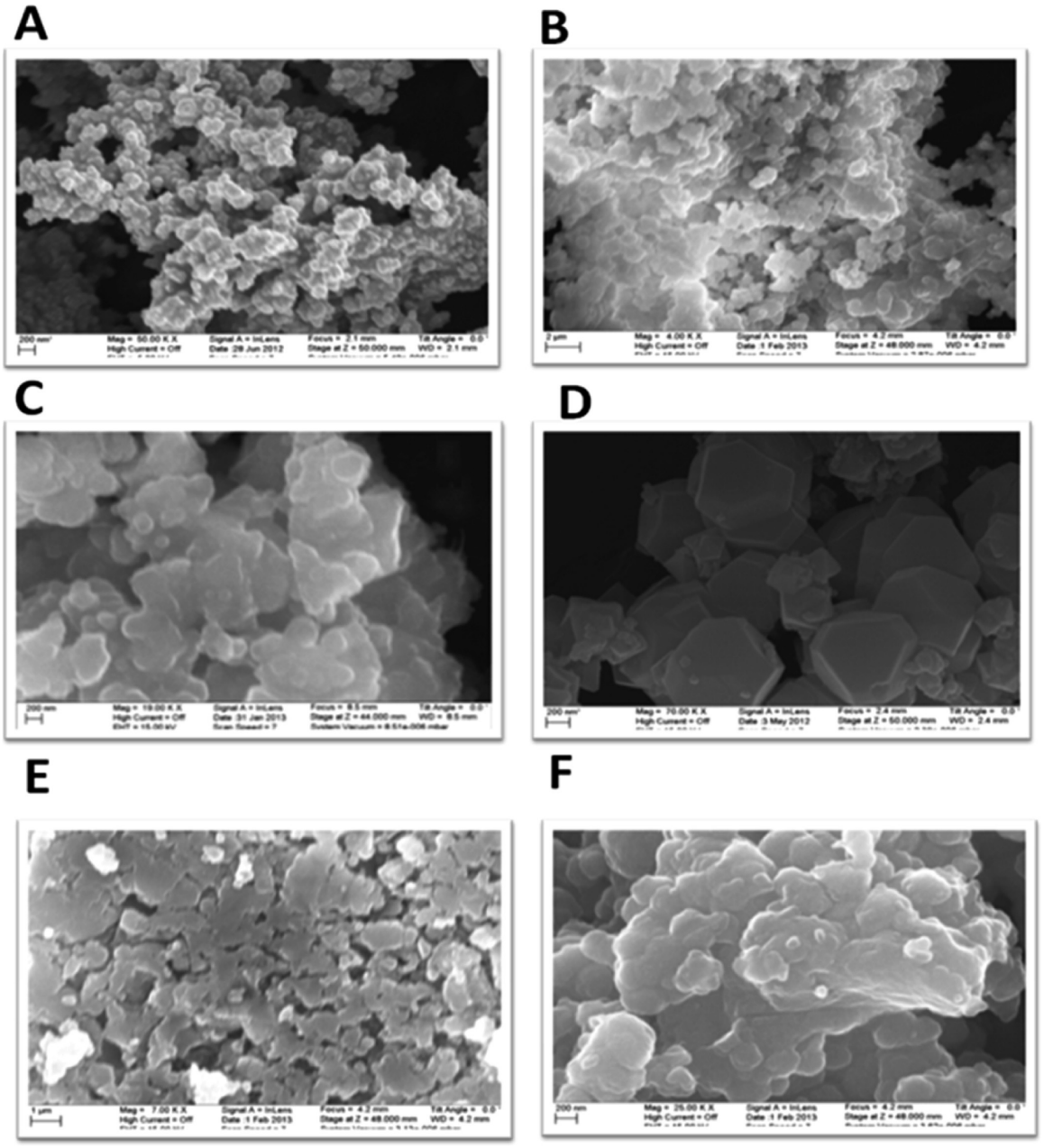

Figure 2. SEM images for UiO-66 (A−C) and UiO-67 (D−F) with and without the incorporation of Ce^{+3}.

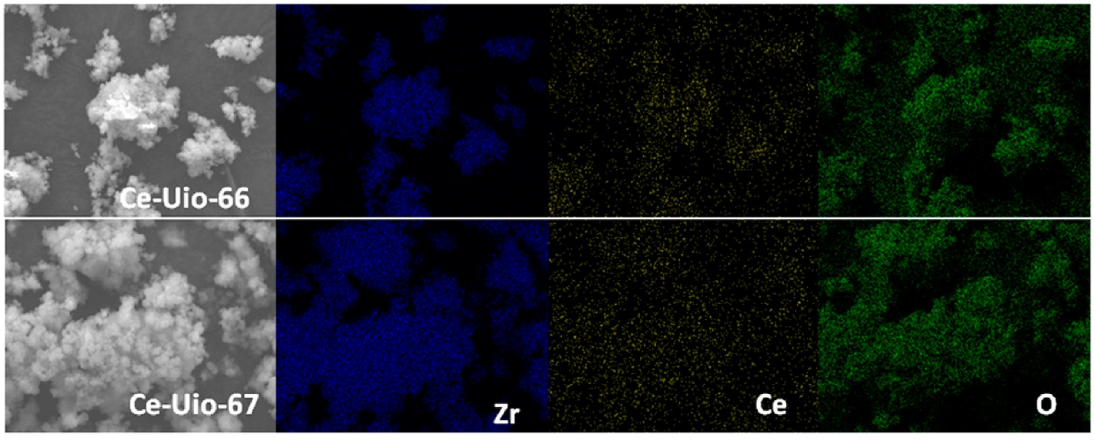

Figure 3. EDX maps for Ce-UiO-66 and Ce-UiO-67.

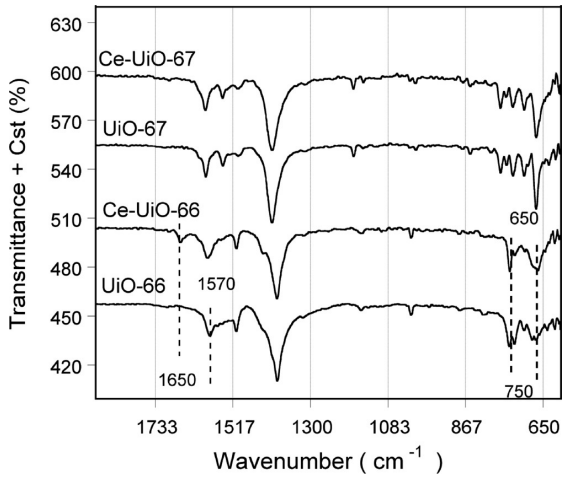

Figure 4. FTIR spectra for the UiO and Ce-UiO series of the samples.

Table 1. NO_2 Adsorption Capacities (mg/g_{ads}), Amounts of Water Adsorbed, and pH Values before and after Exposure to NO_2 in Moist (EM) and Dry (ED) Conditions[a]

			pH	
samples	NO_2 capacity (mg/g_{ads})	water adsorbed (%)	initial	exhausted
UiO-66 ED	73		3.00	2.90
Ce-UiO-66 ED	95		3.64	3.44
UiO-66 EM	40	1.2	3.00	2.88
Ce-UiO-66 EM	53	10.3	3.64	2.52
UiO-67 ED	79		4.78	3.34
Ce-UiO-67 ED	86		3.69	3.39
UiO-67 EM	118	7.2	4.78	2.87
Ce-UiO-67 EM	85	2.0	3.69	3.41

[a]The data for UiO-66 and UiO-67 is taken form ref 18.

nature of our materials. A marked increase in the surface area and the development of porosity are a result of Ce(+3) doping into the MOF (UiO-66/67). In comparison with the structural parameters of the parent UiO-67, the surface area of Ce-UiO-67 and its total pore volume increased more than 67% and 60%, respectively. Interestingly, a detected increase in the micropore volume is only about 15%. Comparing to the unmodified sample, an increase in the surface area and pore volume of about 16% and 9%, respectively, is also found for Ce-UiO-66. The increase in the volume of micropores for this material similar to that found for Ce-UiO-67 (14%). The differences in the surface areas and pore volume between UiO-66 and UiO-67 are the result of the different ligand sizes, and this aspect was discussed in detail elsewhere.[18] The dramatic increase in the surface area and pore volume for Ce-UiO-67 must be the result of the presence of the crystal defects/new phase formed owing to the cerium doping. This process apparently results in the formation of the high volume of mesopores, which are likely small in size since the increase in the surface area is very significant. The small change in the micropore volume can be the result of cerium binding to free carboxylic ligands, which leads to the formation of chelates and thus restricts an access of nitrogen to the MOF cages. It is also possible that Ce^{+3} creates subnanometer particles deposited within the structure of the parent MOF. The effect of cerium on the porosity of Ce-Ui-66 is less visible owing to the limitation in the numbers of carboxylic groups available for reactions with metal cations.

The impact of the Ce^{+3} incorporation into the MOFs structure and chemistry should affect the adsorption/reactive adsorption performance of these materials in the process of NO_2 separation from ambient air in both moist and dry conditions. The measured NO_2 breakthrough curves and desorption curves are shown in Figure 5. The breakthrough

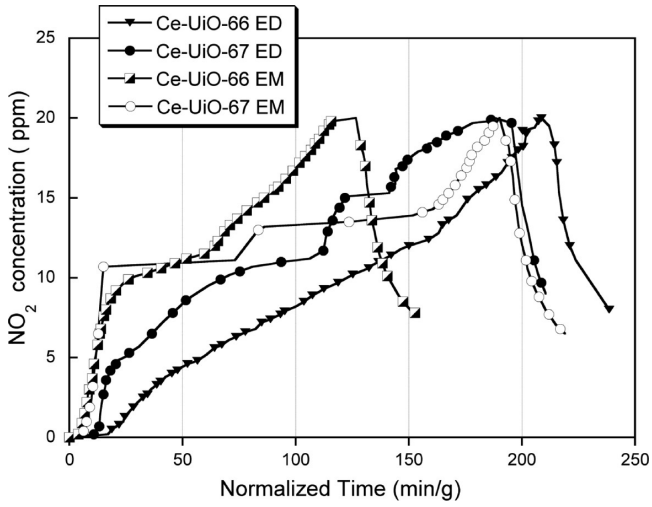

Figure 5. NO_2 breakthrough curves for the Ce-UiO-66 and Ce-UiO-67 samples.

curves reveal several steps. These steps must be related to the changes in the surface chemistry and/or porosity, which affect the dynamics of NO_2 adsorption process. Taking into consideration that there was no sign of a pressure drop in our system, we relate these steps to the redox cycle (Ce^{+4}/Ce^{+3}).[38−40] It is likely that Ce^{+3} is oxidized by NO_2 and thus by formation of Ce^{+4} more active sites for binding NO_2 appear on the surface. This effect is clearly seen for Ce-UiO-67 and for Ce-UiO-66 only small changes in the "normal" shape of the UiO-66 breakthrough curves are detected in dry conditions.[18] In moist conditions the presence of a small, but wide step is seen for Ce-UiO-66 exposed to NO_2. Thus, the presence of moisture facilitates the changes in the framework chemistry.

The influence of the Ce^{+3} doping can be also seen in the NO release curves (Figure 6). Comparing these curves to those for the parent MOFs, it is found that the most noticeable changes are visible for Ce-UiO-67 EM and Ce-UiO-66 EM. In the former case, the duration of the experiment to reach the sensors upper limit doubles compared to other samples, while in the latter case the duration of the experiment decreases 33%.[18] Thus, the presence of water limits the amount of NO released, when unoccupied cationic species are present in the MOF.

The NO_2 breakthrough capacities calculated from the breakthrough curves are compared in Figure 7. The incorporation of Ce^{+3} in MOF has a favorable effect on the adsorption capacities. The performance of the doped materials is better than those of the parent samples regardless the conditions, with the exception of Ce-UiO-67 exposed to NO_2 in moist conditions. In dry conditions, Ce-UiO-66 adsorbs 95 mg/g, which is 30% higher than the amount adsorbed on UiO-66. When water is present in the challenge gas, Ce-UiO-66 is only able to adsorb 53 mg/g; nonetheless, this capacity is 32% higher than that of its parent MOF. In the case of Ce-UiO-67, the NO_2 adsorption capacities are similar in both moist and dry conditions. An important aspect is the percentage of NO

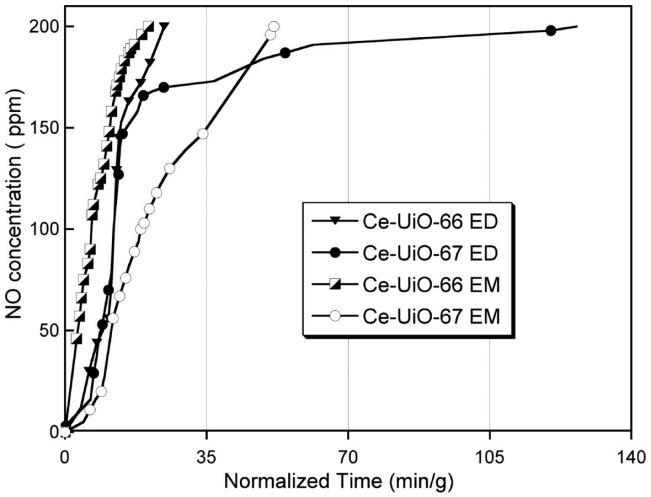

Figure 6. NO release curves for the Ce-UiO-66 and Ce-UiO-67 samples.

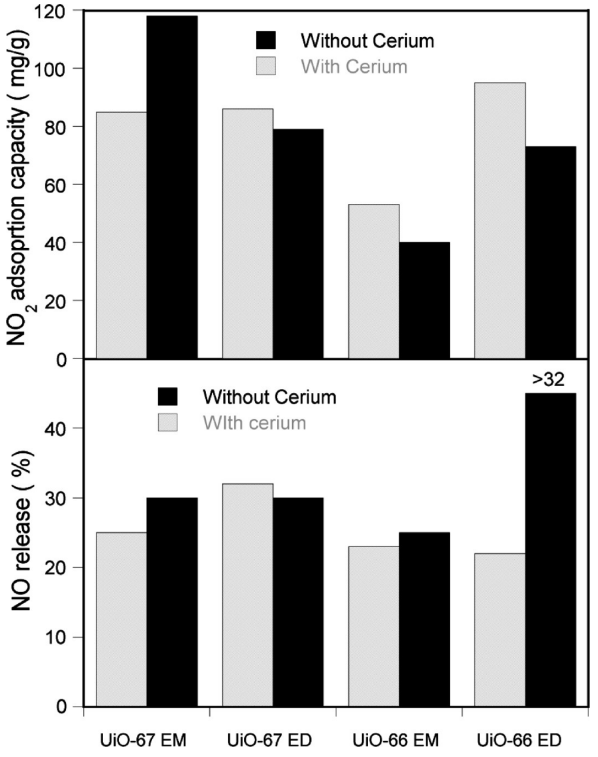

Figure 7. Comparison of the NO_2 adsorption capacity (mg/g) and NO release (%) for materials with and without cerium used in both moist and dry conditions.

released. In the ideal situation, a zero NO release would be desired. Analyzing both, NO_2 adsorption capacity and the percentage of NO released indicates the cerium doping is the most beneficial for UiO-66 when exposed to dry gas. Also, in moist conditions, addition of cerium to UiO-66 increases NO_2 capacity with the decease in NO release. In the case of Ce-UiO-67, parallel changes are found regarding the NO_2 adsorption and NO release.

It was found that the addition of Ce^{+3} cations affects the average surface pH and the ability of these materials to adsorb water. While the former feature significantly increases for Ce-UiO-66 from 3.00 for UiO-66 to 3.64, for Ce-UiO-67 a marked decrease is found in comparison with the parent MOF (3.69 compared to 4.78 for UiO-67). This supports the hypothesis about the neutralization of carboxylic groups by their reaction with cerium during the synthesis of the latter material. On Ce-UiO-67, only 2.0% water was adsorbed during prehumidification in comparison with 7.5% adsorbed on UiO-67.[18] This indicates the limits in the accessibility of pores, likely owing to the formation of chelates. On the other hand, the opposite trend is found for Ce-UiO-66 in the amount of water adsorbed. For this sample an increase from 1.2% to 10.3% in comparison with the undoped counterpart was measured. The two opposite trends in the pH value and water affinity must result in that apparent effects of unchanged adsorption of NO_2 on the latter sample compared to UiO-67. The less acidic pH and the high ability to retain water were found previously to be important factors for NO_2 adsorption on this kind of materials.

The NO_2 adsorption visibly affects the porosity of our samples (Table 2). The pore size distributions of the modified initial and exhausted UiO materials are shown in Figure 8. Interestingly, the average pore diameter for Ce-UiO-67 is around 12 Å, while that of Ce-UiO-66 is around 15 Å, even though the latter sample has a small ligand size. Thus, either Ce^{3+} doping causes expansion of the MOF crystal unit for Ce-UiO-66, or it partially initiates the growth of a cerium based MOF or hybrid MOF, as suggested by changes in the XRD peaks. On the other hand, the small average pore size for Ce-UiO-67 can be the result of the reaction of Ce with carboxylic moiety, which limits the access of nitrogen molecules to the UiO-67 MOF cavities. The importance of pores with sizes between 10 and 25 Å for the process of NO_2 removal is supported by the decrease in their incremental pore volume after exposure to NO_2 in both moist and dry conditions. The most pronounced changes in the porosity are found for Ce-UiO-67 EM and for Ce-UiO-66 ED. The surface areas for these two samples decrease 75% after exposure to NO_2. This indicates that on these two materials the mechanisms of NO_2 adsorption are distinctly different and also different from those on Ce-UiO-66 EM and Ce-UiO-67 ED. While on the latter two samples the physisorption seems to be the predominant mechanism, even in moist conditions, on the Ce-UiO-67 EM and for Ce-UiO-66 ED, reactive adsorption must result in the collapse of these MOFs' frameworks. While in the case of Ce-UiO-66 EM water adsorbed in the chemically modified cavities of the hybrid MOF shields the metals centers from reacting with NO_2, its lack on the surface of Ce-UiO-67 ED combined

Table 2. Parameters of the Porous Structure Derived from the Nitrogen Adsorption Isotherm for the Samples before and after Exposure to NO_2 and the Zr/Ce Atomic Ratio from EDX Analysis[a]

sample	S_{BET} [m^2/g]	V_t [cm^3/g]	V_{mic} [cm^3/g]	V_{mic}/V_t	Zr/Ce [in atom %]
UiO-66	891	0.471	0.391	0.83	
Ce-UiO-66	1035	0.515	0.445	0.86	13
Ce-UiO-66 ED	273	0.143	0.102	0.71	
Ce-UiO-66 EM	1027	0.507	0.443	0.87	
UiO-67	1372	0.707	0.608	0.86	
Ce-UiO-67	2302	1.133	0.705	0.62	46
Ce-UiO-67 ED	2197	1.048	0.694	0.66	
Ce-UiO-67 EM	628	0.316	0.204	0.64	

[a]The data for UiO-66 and UiO-67 is taken form ref 18.

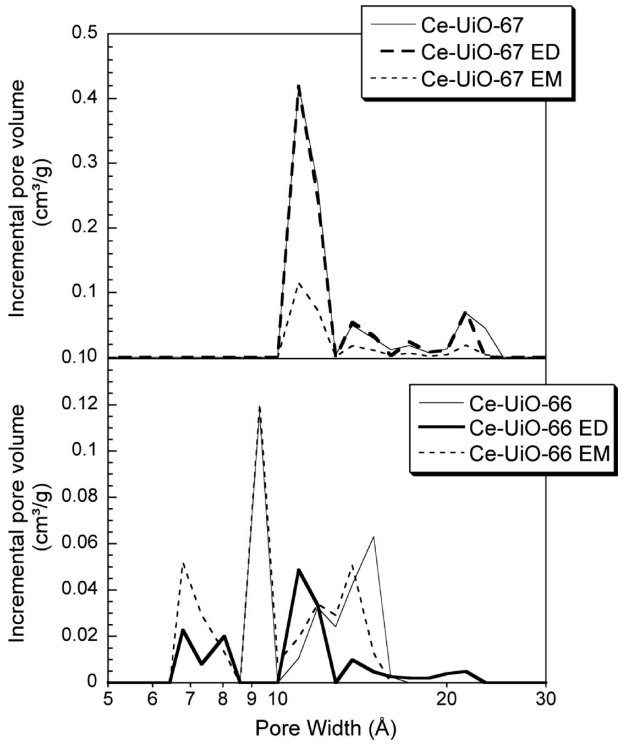

Figure 8. Pore size distributions for Ce-UiO-66 and Ce-UiO-67 before and after exposure to NO_2.

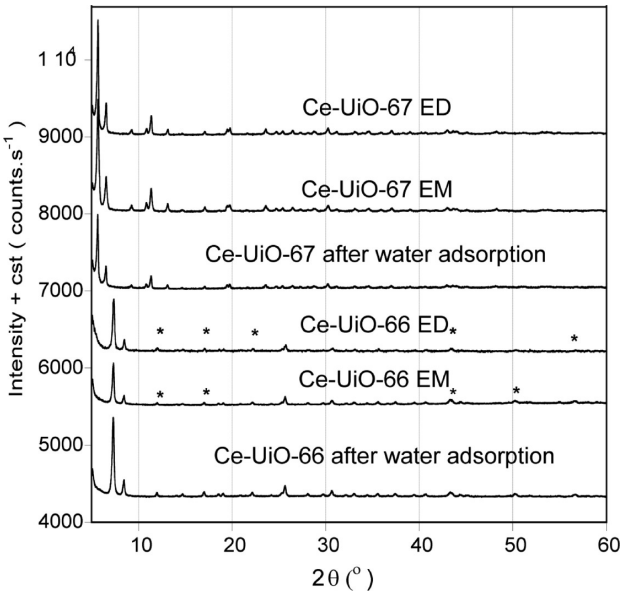

Figure 9. XRD patterns for the exhausted samples. The peaks discussed in the text are marked with an asterisk (*).

with the limited access to metal centers owing to the chelation of cerium with carboxylic groups of the linkages result in the stability of the framework.[18] The collapse of the framework in the case of Ce-UiO-67 EM is the effect of dissociation of the cerium from its binding with COOH moieties, which leads to the opening of the cavities and thus enable a direct attack of the nitrous/nitric acids, formed in the water film, on the metal centers. Another factor which might contribute to the observed behavior is instability of UiO MOF when exposed to water. It has been recently reported that water has a detrimental effect on the structure of these material and especially on UiO-67.[41] In this MOF, the instability of biphenyl ring leading to the collapse of the porous network was linked to torsional strain/rotational effects in its crystalline structure. In the case of Ce-UiO-66 ED, owing to the lack of water, the metal centers in the small pores are not shielded and react with NO_2. The whole adsorption process is very dynamic since Ce^{+3} is likely oxidized by NO_2 to Ce^{+4} and thus more adsorption centers for nitrates are formed. Nevertheless, the collapse of the structure has a negative effect on the overall performance of Ce-UiO-67 in moist conditions and of Ce-UiO-66 in dry conditions as NO_2 adsorbents. It also crosses out the possibility of their application after a simple regeneration treatment/desorption. The high release of NO from Ce-UiO-66 ED supports reduction of NO_2 on cerium centers of this adsorbent (Figure 7).

The XRD patterns for the exhausted samples are collected in Figure 9. The previous studies indicated that in the case of reactive adsorption a decrease or disappearance of XRD peaks is expected after the exposure to toxic gases, which is due to the partial or complete destruction of the MOF structure.[42,43] The partial destruction of crystallinity is specifically visible for Ce-UiO-66 ED and Ce-UiO-66 EM. Moreover, a new peak appears at 2θ = 9.4° for Ce-UiO-66 exposed to NO_2 in moist conditions. Contrary to the case of Ce-UiO-66, the X-ray diffraction pattern for Ce-UiO-67 reveals a decrease in its main diffraction peaks at 2θ values of 10°, 12°, 20°, and 31.5° after exposure to NO_2 in both conditions. This is consistent with the observed changes in the porosity. New peaks after exposure to NO_2 in dry conditions are visible but are of very small intensity. These peaks are linked to cerium nitrate.[44] In the case of Ce-UiO-67 EM, a slight shift in the peak at 2θ value of 5.8 occurs. This can be caused by some structural rearrangements of the framework to accommodate NO_2 molecules and by torsional strains mentioned above.[41]

Owing to the chemistry involved, gas−solid interactions lead to the formation of species bound to the surface. Weight loss derivative curves (DTG) for the initial and exhausted materials are collected in Figure 10. The peaks represent weight loss due the decomposition of surface species. The first peak revealed at around 100 °C corresponds to the removal of moisture. Doping with Ce^{+3} results in changes in the weight loss patterns. A small peak seen between 100 and 150°C is related to the presence of hydroxylated Ce^{+3} species in the framework.[45−47] Since the drying process applied was rather long and the solvent is expected to be removed, a small peak between 200 and 300 °C represents the decomposition of organic ligands metallically coordinated to cerium and the formation of the crystalline phase of Ce_2O.[33,48,49] A peak between 400 and 500°C is shifted to 550 °C. It corresponds to the decomposition of the framework and the removal of organic ligands linked to the zirconium, and/or cerium metallic centers. Thus, it is apparent that cerium (+3) doping improves the thermal stability of these MOFs. The wide shoulder present for UiO-67 between 500 and 600 °C disappears for UiO-67 doped with Ce^{+3}. Additionally, small peaks are visible on the DTG curves between 600 and 800°C on the cerium (+3) doped MOF. They are ascribed to the decomposition of Ce_2O_3.[48] After exposure to NO_2, the peaks on the DTG curves between 100 and 190 °C increase in their intensity for Ce-UiO-66 EM and Ce-UiO-67 ED are ascribed to the decomposition of cerium (+3) nitrate hydrate.[50] The intense peak at 100 °C for Ce-UiO-66 in moist conditions is linked to the presence of water. The intensity of the peak revealed between 200 and 350 °C increases in both

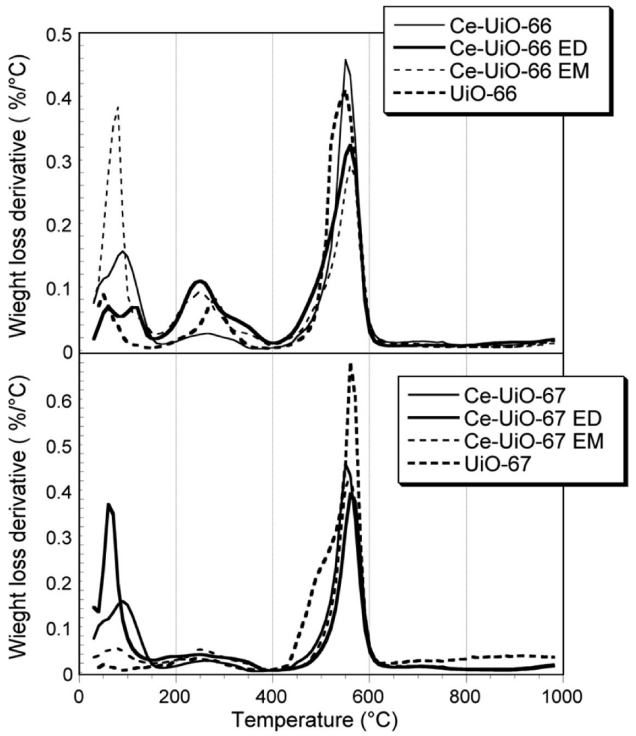

Figure 10. DTG curves in nitrogen for the exhausted samples.

moist and dry conditions for Ce-UiO-66. In moist conditions, this peak is linked to the decomposition of ZrO−(OH)−NO_2, CeO−(OH)−NO_2 acidic complexes,[51] whereas in dry conditions it is linked to the decomposition of metal nitrates (zirconium or cerium).[52−55] Interestingly, a shoulder appears around 350−400 °C after NO_2 adsorption in both conditions. We link this new feature to the formation of nitrates/nitrites bound to the ceria centers.[56]

Additional information about the nature of the species deposited on the surface after exposure to NO_2 is provided by FTIR spectroscopy carried out on the exhausted samples (Figure 11). A broadening of a band positioned at 750 cm^{-1} is visible for Ce-UiO-66 exposed to NO_2 in both moist and dry conditions. This band is linked to symmetric and asymmetric vibration of NO_2 (*v*s and *v*a (NO_2).[57] The intensity of the

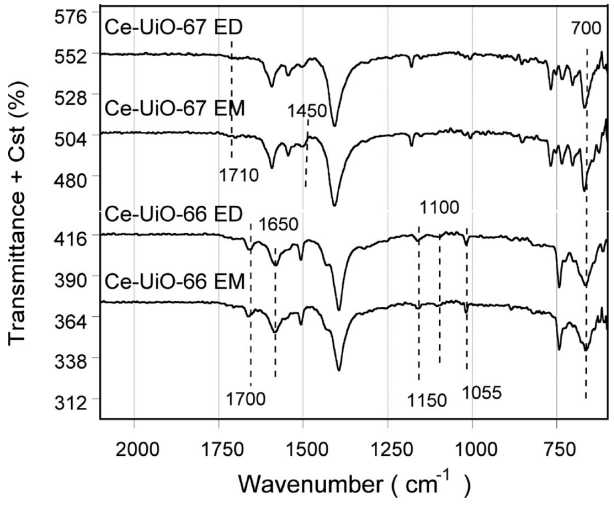

Figure 11. FTIR spectra for the exhausted samples.

bands around 850 and 1055 cm^{-1} also slightly increases. The former is linked to the weakly chemisorbed NO_2, while the latter is related to monodentate nitrate *v*(NO) vibration.[54] Additionally, the bands between 1100 and 1150 cm^{-1} broaden after exposure to NO_2 in both moist and dry conditions. We link these changes either to the direct interactions of NO_2 with C−O or the interactions of NO_2 with metal coordinated species (Ce−O−C). Moreover, the band related to the formation of nitrate and nitrates species[58] at around 1650 cm^{-1} broadens and slightly decreases in its intensity. Typical vibration for Ce^{+4}−NO_2, Ce^{+3}−NO_2 occur around this wave number.[59] This indicates that NO_2 is chemically linked to the free Ce^{+3} centers and results in the formation of cerium (+3/+4) nitrate species. In addition, on the spectrum for Ce-UiO-66 exposed to NO_2 in moist conditions, the bands in the range between 1300 and 1400 cm^{-1} become smoother. The decrease in the intensity of these bands indicates the consumption of the benzene rings during the nitration reaction.[18]

Interestingly, Ce-UiO-67 exposed to NO_2 in both conditions does not exhibit any well pronounced changes on the FTIR spectra. Nonetheless, the band at 750 cm^{-1} broadens and decreases in intensity after adsorption and a weak spectral band appears between 1650 and 1750 cm^{-1}, which we link to formation of nitrate and nitrite species.

CONCLUSIONS

The influence of Ce^{+3} doping on the alteration of Zr-MOF surface features has been demonstrated based on the results of various analytical techniques discussed above. The potential application of this adsorbent for gas separation and breathing air filtration in ambient conditions is promising. Doping with cerium not only results in the development of porosity, but it also increases the structural stability and resistance to the corrosive effects of NO_2. Although the crystal structures are strikingly different from those of their parent materials, doping UiO with cerium leads to formation of surface chemistry favorable for NO_2 reactive adsorption. The results indicate that the hybrid Ce−Zr MOF phase is formed when the number of carboxylic reactive ligands is limited as that in BDC. On the hand, in the case of BDPC linkages, Ce^{+3} reacts with carboxylic groups, causing spatial limitations in the accessibility of small pores for water and adsorbate molecules. The increase in NO_2 adsorption is linked to (Ce^{+4}/Ce^{+3}) redox cycle and thus to the formation of more active centers for NO_2 binding. The doping process also leads to the formation of new micropores as a result of an increase in surface heterogeneity and imperfection of crystals. These micropores enhance NO_2 adsorption. The preservation of the characteristic diffraction peaks after exposure to NO_2 indicates the overall stability of Ce-UiO materials. Nitric and nitrous acid formed by dissolution of NO_2 in the water film and subsequent nitration of the biphenyl rings contribute to major loss in the porosity in Ce-UiO-67 EM.

AUTHOR INFORMATION

Corresponding Author

*Tel: (212)650-6017. Fax: (212)650-6107. E-mail: tbandosz@ccny.cuny.edu.

Notes

The authors declare no competing financial interest.

■ ACKNOWLEDGMENTS

This study was supported by the ARO (Army Research Office) Grant W911NF-10-1-0030 and NSF collaborative SBET Grant No. 1133112. The authors are grateful to Mr. Albert Tamashausky of Asbury Carbon for his help with ICP analysis.

■ REFERENCES

(1) Karra, J. R.; Grabicka, B. E.; Huang, Y.-G.; Walton, K. S. *J. Colloid Interface Sci.* **2013**, *392*, 331−336.
(2) Zhao, Z.; Li, Z.; Lin, Y. S. *Ind. Eng. Chem. Res.* **2009**, *48*, 10015−10020.
(3) Li, Y.; Yang, R. T. *Langmuir* **2007**, *23*, 12937−12944.
(4) Saha, D.; Bao, Z.; Jia, F.; Deng, S. *Environ. Sci. Technol.* **2010**, *44*, 1820−1826.
(5) Anbia, M.; Hoseini, V.; Sheykhi, S. *J. Ind. Eng. Chem.* **2012**, *18*, 1149−1152.
(6) Bao, Z.; Yu, L.; Ren, Q.; Lu, X.; Deng, S. *J. Colloid Interface Sci.* **2011**, *353*, 549−556.
(7) Purewal, J.; Liu, D.; Sudik, A.; Veenstra, M.; Yang, J.; Maurer, S.; Müller, U.; Siegel, D. J. *J. Phys. Chem. C* **2012**, *116*, 20199−20212.
(8) Saha, D.; Zacharia, R.; Lafi, L.; Cossement, D.; Chahine, R. *Chem. Eng. J.* **2011**, *171*, 517−525.
(9) Heymans, N.; Vaesen, S.; De Weireld, G. *Microporous Mesoporous Mater.* **2012**, *154*, 93−99.
(10) Saha, D.; Deng, S. *J. Colloid Interface Sci.* **2010**, *348*, 615−620.
(11) Petit, C.; Mendoza, B.; Bandosz, T. J. *Langmuir* **2010**, *26*, 15302−15309.
(12) Petit, C.; Huang, L.; Jagiello, J.; Kenvin, J.; Gubbins, K. E.; Bandosz, T. J. *Langmuir* **2011**, *27*, 13043−13051.
(13) Petit, C.; Bandosz, T. J. *Adv. Funct. Mater.* **2010**, *20*, 111−118.
(14) Petit, C.; Bandosz, T. J. *J. Mater. Chem.* **2009**, *19*, 6521−6528.
(15) Bandosz, T.; Petit, C. *Adsorption* **2011**, *17*, 5−16.
(16) Petit, C.; Levasseur, B.; Mendoza, B.; Bandosz, T. J. *Microporous Mesoporous Mater.* **2012**, *154*, 107−112.
(17) Cavka, J. H.; Jakobsen, S.; Olsbye, U.; Guillou, N.; Lamberti, C.; Bordiga, S.; Lillerud, K. P. *J. Am. Chem. Soc.* **2008**, *130*, 13850−13851.
(18) Ebrahim, A. M.; Levasseur, B.; Bandosz, T. J. *Langmuir* **2012**, *29*, 168−174.
(19) Mavrandonakis, A.; Tylianakis, E.; Stubos, A. K.; Froudakis, G. E. *J. Phys. Chem. C* **2008**, *112*, 7290−7294.
(20) Mulfort, K. L.; Wilson, T. M.; Wasielewski, M. R.; Hupp, J. T. *Langmuir* **2008**, *25*, 503−508.
(21) Dalach, P.; Frost, H.; Snurr, R. Q.; Ellis, D. E. *J. Phys. Chem. C* **2008**, *112*, 9278−9284.
(22) Ghoufi, A.; Deschamps, J.; Maurin, G. *J. Phys. Chem. C* **2012**, *116*, 10504−10509.
(23) Kubo, M.; Shimojima, A.; Okubo, T. *J. Phys. Chem. C* **2012**, *116*, 10260−10265.
(24) Mavrandonakis, A.; Klontzas, E.; Tylianakis, E.; Froudakis, G. E. *J. Am. Chem. Soc.* **2009**, *131*, 13410−13414.
(25) Chu, C.-L.; Chen, J.-R.; Lee, T.-Y. *Int. J. Hydrogen Energy* **2012**, *37*, 6721−6726.
(26) Bae, Y.-S.; Hauser, B. G.; Farha, O. K.; Hupp, J. T.; Snurr, R. Q. *Microporous Mesoporous Mater.* **2011**, *141*, 231−235.
(27) Murakami, M.; Hong, D.; Suenobu, T.; Yamaguchi, S.; Ogura, T.; Fukuzumi, S. *J. Am. Chem. Soc.* **2011**, *133*, 11605−11613.
(28) Imagawa, H.; Suda, A.; Yamamura, K.; Sun, S. *J. Phys. Chem. C* **2011**, *115*, 1740−1745.
(29) Lastoskie, C.; Gubbins, K. E.; Quirke, N. *J. Phys. Chem.* **1993**, *97*, 4786−4796.
(30) Dau, P. V.; Kim, M.; Garibay, S. J.; Münch, F. H. L.; Moore, C. E.; Cohen, S. M. *Inorg. Chem.* **2012**, *51*, 5671−5676.
(31) Chang, N.; Yan, X.-P. *J. Chromatogr., A* **2012**, *1257*, 116−124.
(32) Abid, H. R.; Tian, H.; Ang, H.-M.; Tade, M. O.; Buckley, C. E.; Wang, S. *Chem. Eng. J* **2012**, *187*, 415−420.
(33) Yu, J.-Y.; Wei, W.-C. J.; Lin, S.-E.; Sung, J.-M. *Mater. Chem. Phys.* **2009**, *118*, 410−416.
(34) Nguyen, T. B.; Deloume, J. P.; Perrichon, V. *Appl. Catal ., A* **2003**, *249*, 273−284.
(35) Wang, C.; Xie, Z.; deKrafft, K. E.; Lin, W. *J. Am. Chem. Soc.* **2011**, *133*, 13445−13454.
(36) Valenzano, L.; Civalleri, B.; Chavan, S.; Bordiga, S.; Nilsen, M. H.; Jakobsen, S.; Lillerud, K. P.; Lamberti, C. *Chem. Mater.* **2011**, *23*, 1700−1718.
(37) Ksapabutr, B.; Gulari, E.; Wongkasemjit, S. *Mater. Chem. Phys.* **2004**, *83*, 34−42.
(38) Mitchell, M. B.; Sheinker, V. N.; Tesfamichael, A. B.; Gatimu, E. N.; Nunley, M. *J. Phys. Chem. B* **2002**, *107*, 580−586.
(39) Levasseur, B.; Ebrahim, A. M.; Bandosz, T. J. *Langmuir* **2011**, *27*, 9379−9386.
(40) Bamwenda, G. R.; Uesigi, T.; Abe, Y.; Sayama, K.; Arakawa, H. *Appl. Catal., A* **2001**, *205*, 117−128.
(41) DeCoste, J.B.; Peterson, G.W.; Jasuja, H.; Glover, T.G.; Huang, Y.-G.; Walton, K.S. *J. Mater. Chem. A* **2013**, *1*, 5642−5650.
(42) Levasseur, B.; Petit, C.; Bandosz, T. J. *ACS Appl. Mater. Interfaces* **2010**, *2*, 3606−3613.
(43) Petit, C.; Mendoza, B.; O'Donnell, D.; Bandosz, T. J. *Langmuir* **2011**, *27*, 10234−10242.
(44) Ruas, A.; Simonin, J.-P.; Turq, P.; Moisy, P. *J. Phys. Chem. B* **2005**, *109*, 23043−23050.
(45) Cui, M. Y.; He, J. X.; Lu, N. P.; Zheng, Y. Y.; Dong, W. J.; Tang, W. H.; Chen, B. Y.; Li, C. R. *Mater. Chem. Phys.* **2010**, *121*, 314−319.
(46) Cui, Q.; Dong, X.; Wang, J.; Li, M. *J. Rare Earths* **2008**, *26*, 664−669.
(47) Ksapabutr, B.; Gulari, E.; Wongkasemjit, S. *Mater. Chem. Phys.* **2006**, *99*, 318−324.
(48) Lu, C.-H.; Wang, H.-C. J. *Mater. Sci. Eng., B* **2002**, *90*, 138−141.
(49) Sun, C.-Y.; Hu, S.-L.; Xing, H.-T.; Dong, C.-M.; Zhan, Z.-S. *Chin. J. Appl. Chem* **2010**, *27*, 1172−1176.
(50) Vratny, F.; Kern, S.; Gugliotta, F. *J. Inorg. Nucl. Chem.* **1961**, *17*, 281−285.
(51) Strydom, C. A.; Vuuren, C. P. J. *J. Therm. Anal.* **1987**, *32*, 157−160.
(52) Silva, G. L. J. P. d. *Mater. Res.* **2002**, *5*, 149−153.
(53) Stefani, G.; Grzeta, B.; Popovic, S.; Music, S. *Croat. Chem. Acta.* **1999**, *72*, 395−412.
(54) Mohamed, G. G.; Soliman, A. A.; El-Mawgood, M. A. *Spectrochim. Acta, Part A* **2005**, *62*, 1095−1101.
(55) Nibha Kapoor, I. P. S.; Singh, G.; Frohlich, R. *J. Mol. Struct.* **2013**, *1034*, 296−301.
(56) Miguel-García, I.; Parres-Esclapez, S.; Lozano-Castelló, D.; Bueno-López, A. *Catal. Commun.* **2010**, *11*, 848−852.
(57) Wang, J.; Koel, B. E. *J. Phys. Chem. A* **1998**, *102*, 8573−8579.
(58) Wang, Z.-M.; Arai, T.; Kumagai, M. *Ind. Eng. Chem. Res.* **2001**, *40*, 1864−1871.
(59) Kladis, C.; Bhargava, S. K.; Foger, K.; Akolekar, D. B. *J. Mol. Catal. A: Chem.* **2001**, *171*, 243−249.